WATER RESOURCES RESEARCH, VOL. 26, NO. 3, PAGES 491–500, MARCH 1990

Modeling Fracture Flow With a Stochastic Discrete Fracture Network: Calibration and Validation 2. The Transport Model

M. C. CACAS, E. LEDOUX, AND G. DE MARSILY[1]

Ecole des Mines de Paris, Fontainebleau, France

A. BARBREAU

Commissariat à l'Energie Atomique, Fontenay aux Roses, France

P. CALMELS, B. GAILLARD, AND R. MARGRITTA

Office des Rayonnements Ionisants, Centre d'Etudes Nucléaires de Grenoble, Grenoble, France

As part of the development of a methodology for investigating flow and transport in fractured rocks, a large-scale experiment was recently performed at Fanay-Augères, France. In a companion paper (Cacas et al., this issue) (paper 1) the results of the flow measurements were analyzed. In this paper, the results of the tracer experiments are interpreted. A particle following is coupled to the flow model, described in paper 1. Microscopic dispersion in the fractures and retardation effects due to unevenness of the flow paths are taken into account. The transport model is calibrated on in situ tracer tests, whereas the parameters of the hydraulic model were initially fitted on structural and hydraulic measurements (paper 1). The dispersive properties of the model are reasonably comparable to those of the real site. It tends to confirm the validity of the preliminary hydraulic calibration of the model and thus to validate further the approach used to simulate hydraulic and transport phenomena.

INTRODUCTION AND EXPERIMENTAL SETUP

Cacas et al. [this issue] develop a stochastic and discrete model of flow through fractured media. It is based on the representation of the flow pattern by a three-dimensional random network of interconnected pipes, whose statistical geometry in inferred from in situ observations. The hydraulic conductivity of these pipes is drawn at random in a lognormal distribution where the parameters are calibrated on a first set of in situ data: local injectivity measurements. This modeling approach was applied to the test site of the Fanay-Augères uranium mine, France.

The calibration of the average pipe conductivities was validated on a second set of measurements concerning the global-scale properties of the medium. In paper 2, we present an attempt at validating the calibration of the variance of these conductivities. To this end, a third set of in situ tests is used: these are tracer tests that characterize the hydrodynamic dispersion in the medium.

The investigated domain is a highly fractured granite surrounding a 100-m-long drift, 150 m below the ground. The experimental site, fully described in paper 1, is recalled here in Figure 1. The tests consists in 10 tracer injections [*Calmels et al.*, 1986] performed in 5-m-long packed-chambers located along boreholes F2 and F3 (see Figure 1). Six injections of different chemicals were performed first in chambers 1-F1 (1-F1 means chamber 1 of borehole F1) (zinc ethylene-diamine-tetraacetic acid (EDTA), 0.4 kg), 4-F2 (fluoresceine, 0.09 kg), 6-F2 (nickel EDTA, 0.025 kg), 7-F2 (iodine NaI, 0.48 kg), 4-F3 (rhodamine WT, 1.10^{-4} m^3), and 7-F3 (amino G, 0.1 kg). A second measurement campaign was carried out after the previously injected chemicals had totally disappeared from the medium. The four chambers 3-F2, 1-F3, 3-F3, and 6-F3 were injected with rhodamine WT (1.10^{-4} m^3), iodine NaI (0.05 kg), amino G (0.05 kg), and zinc EDTA (0.25 kg), respectively. These tracers are assumed to be chemically stable and not to react with the medium.

The tracers were put in the chambers and then forced into the medium by injection of additional fresh water. No significant pressure increase was noticed during these injections. The tracer concentration of the water seeping through the drift was monitored by analyzing water samples taken at three locations as indicated in Figure 1: (1) at the roof of the gallery, precisely at the level of the injection section in a plastic sheet attached to the rock (location A), (2) in the drain collecting the water flowing to the gallery, from 0 to 25 m downstream from the injection section (location B), and (3) in the drain, from 25 to 50 m downstream from the injection section (location C).

Samples were also taken in boreholes F1 and F4 at 5, 12, and 18 m from the tunnel, showing that tracer transport also occurs in the direction parallel to the drift. A rhodamine WT concentration profile along the drift in the drain collecting seepage water was established 2 weeks after the chemical was injected in chamber 4-F3 (see Figure 2). This profile shows that the tracer influx into the gallery is concentrated at three influx locations.

The 10 injection experiments yielded erratic results: (1)

[1]Also at Université Pierre et Marie Curie, Paris VI, France.

Paper number 89WR03133.
0043-1397/90/89WR-03133$05.00

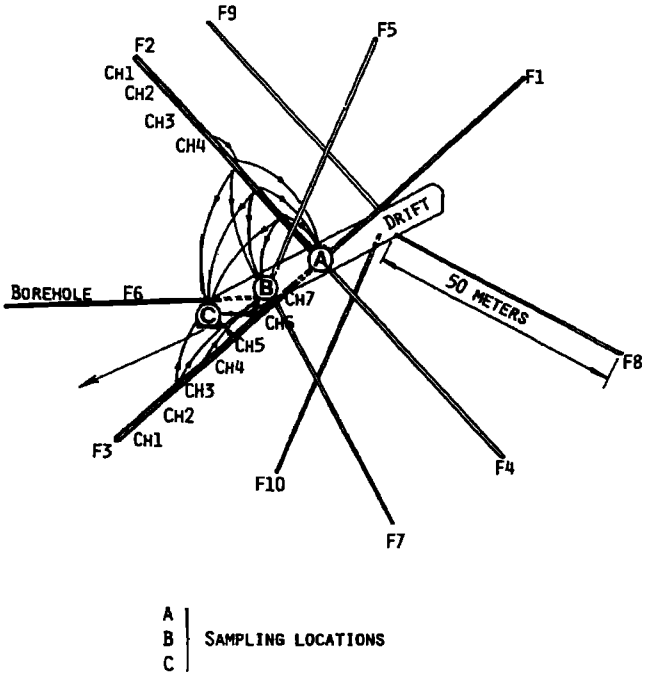

Fig. 1. Description of the tracer tests performed in Fanay-Augeres.

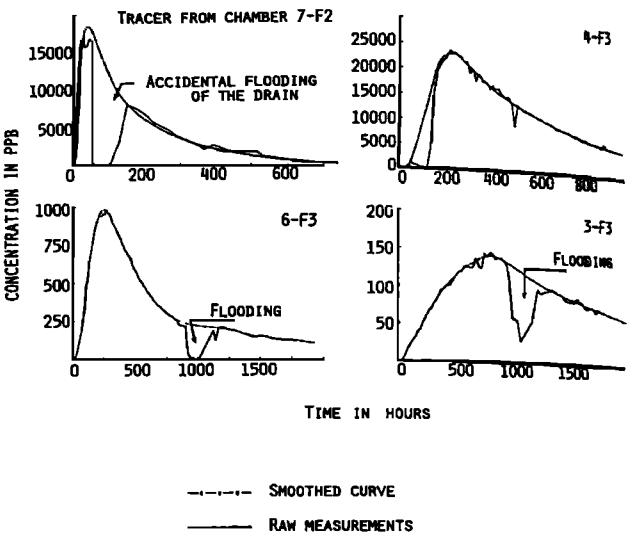

Fig. 3. Breakthrough curves observed at the collecting point B.

the tracer stagnated in chamber 1-F2; (2) the tracers injected in chambers 3-F2 and 1-F1 were never recovered in the drift, due to lateral flow; (3) injection in chamnber 7-F3 was disturbed by a technical failure; and (4) the breakthrough of the tracer injected in chamber 5-F2 was multimodal and rather difficult to interpret; however, this is not surprising in a fractured medium.

Only the five injections in chambers 6-F2, 7-F2, 4-F3, 6-F3, and 3-F3 led to unquestionable breakthroughs but with various time scales. The breakthrough curves of the tracers recovered in the central part of the drift (location B) are presented in Figure 3. These curves are peak-shaped with a long tail but appear relatively smooth. We will characterize them later by two quantities: the time of peak arrival and the total breakthrough duration. We defined this breakthrough duration as the time elapsed between the first tracer arrival and the breakthrough time for a tail concentration equal to 5% of the peak concentration. The times of the peak of arrival and the breakthrough durations of the different injection experiments are given in Table 1.

The tracer breakthroughs are also characterized by the very low percentage of tracer that returned to the drift (Table 1). Even for the tracer injected chamber 7-F2, 10 m from the drift, only 45% was collected in the drain.

These tracer tests characterize the main features of the macroscopic dispersion occurring in the investigated domain: a very broad distribution of tracer velocity (long tails of recovery) and channellized migrations (punctual inflows along the drift).

Since the granite matrix has extremely low porosity and permeability and since the tracer tests only involve short time scales, the tracer motion is almost entirely due to advection through the fracture network, and matrix diffusion can be neglected. It is basically the flow velocity field (and the corresponding hydrodynamic dispersion) that governs the tracer migration. Thus, if a particle advection simulator based on the flow pattern obtained from our hydraulic model is able to account for the observed dispersive properties mentioned previously, then we can conclude that this hydraulic model is satisfactory. This is our objective. We intend to develop a particle advection model based on our stochastic discrete flow model described in paper 1. Then, by comparing tracer test simulations and the tracer experiments, we can establish whether the basic flow pattern is adequate or not, i.e., whether our flow modeling approach is valid or not.

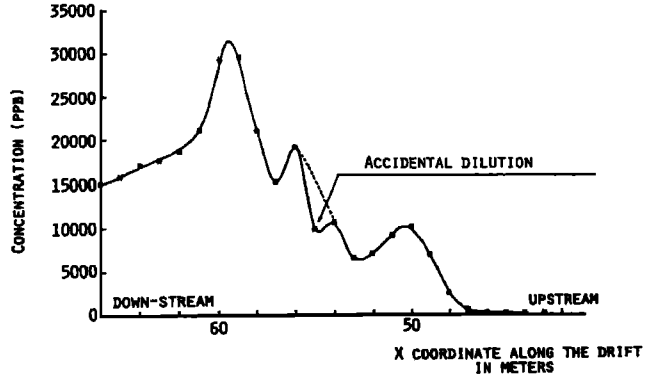

Fig. 2. Rhodamine WT Profile along the drift in the drain collecting seepage water.

PARTICLE ADVECTION MODEL

A description of the basic flow modeling technique can be found in paper 1. The flow computation yields the velocity distribution over a three-dimensional random network of linear elements or "pipes" (Figure 4). These elements are a conceptual model of the flow paths in the fractures. The connections between the pipes, called "nodes," represent the fracture centers.

At least two approaches can be considered when simulating transport through such a network of "pipes." The first one (presented, e.g., by *Roux et al.* [1986]) consists of solving the convection-diffusion equation in each element of

TABLE 1. Main Results of the Injection Experiments

Injection Chamber	Tracer	Time of the Peak Arrival (in hours)	Recovery Rate %	Breakthrough Duration (in hours)
		Collecting Point A		
Iodine (NaI)	F2-Ch7	10.5	13	100
Nickel EDTA	F2-Ch6	12.8	6	160
Fluoresceine	F2-Ch4	29	0.001	unobservable
Rhodamine WT	F2-Ch3	...	...	...
Zinc EDTA	F2-Ch1	...	...	...
		Collecting Point B		
Amino G	F3-Ch7	...	(leakage during injection)	
Zinc EDTA	F3-Ch6	744	14	≃ 4000
Rhodamine WT	F3-Ch4	173	5	≃ 1200
Amino G	F3-Ch3	260	0.009	2000
Iodine NaI	F3-Ch1	...	...	...
Iodine NaI	F2-Ch7	33.5	45	600
Nickel EDTA	F2-Ch6	...	>6	unobservable
Fluoresceine	F2-Ch4	...	>0.001	...
Rhodamine WT	F2-Ch3	...	...	...
Zinc EDTA	F2-Ch1	...	...	...
		Collecting Point C		
Iodine NaI	F2-Ch7	69	6.6	600
Zinc EDTA	F3-Ch6	1080	9	≃ 4000
Rhodamine WT	F3-Ch4	420	0.4	≃ 2000
Amino G	F3-Ch3	600	0.007	≃ 2500

the network and then using a transfer matrix algorithm to convolute the bond responses to the tracer injection. The convolution technique was rejected in this study because it requires the solution of several linear systems of equations with as many unknowns as the number of pipes in the network. The computing efforts required are prohibitive.

The second method consists in discretizing the tracer as a finite number of elementary "particles" representing one or several molecules. The motion of these particles is simulated with an advection-biased random walk technique. This method was used, for example, by *Robinson* [1984], *Schwartz et al.* [1983], *Smith and Schwartz* [1984], and *Tsang and Tsang* [1987]. Various alternatives to this technique were developed. *Schwartz et al.* [1983] used a "particle-tracking" method where time is discretized and particles are indivisible. *Robinson* [1984] proposed both the "mass-lumping" algorithm where time and space are discretized and the particles are split up at the intersections and the "particle-following" method presented below. According to Robinson, this last technique seems to be the fastest one in terms of CPU time. Moreover, it is easily adaptable to the simulation of microscopic hydrodynamic dispersion. For these reasons, it was chosen in our study.

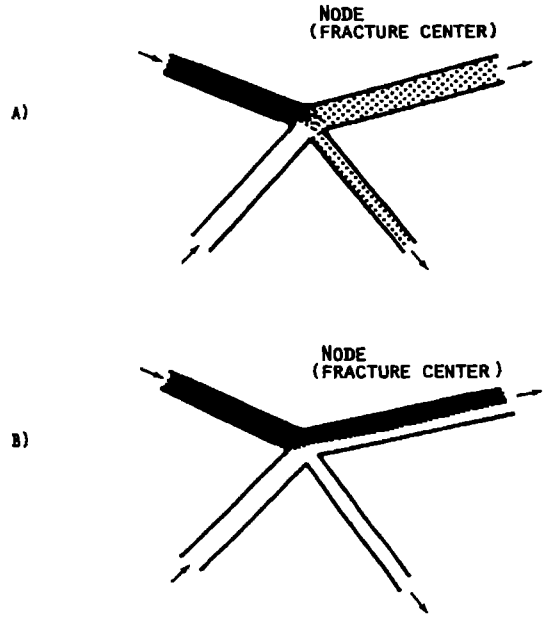

Fig. 4. The network of pipes and the stream tubes. (*a*) With the hypothesis of complete mixing at the intersections. (*b*) With the hypothesis of no mixing at the intersections.

Particle-Following Method

In its original form, the particle-following method consists of following discrete particles added to the flow, whose trajectories are determined from the flow pattern. The main assumptions are the following: (1) the particles are moved by advection only; longitudinal dispersion is neglected; (2) chemical reactions and sorption are not taken into account; and (3) diffusion both in the fluid and the rock matrix is neglected.

The particle trajectories are drawn at random according to the following rules:

1. The particle trajectory is divided into elementary steps corresponding to the displacement between two adjacent connections. An average travel time is computed at each step. It is inferred from the flow rate and the volume of the bond through which the particle travels. The total residence time of a particle along its path is given by the summation of the elementary travel times computed at each step, from the entrance to the exit point.

2. When the particle arrives at a new connection, the next bond through which it is going to move is drawn at

random. The assumption of a perfect mixing of the different fluxes entering a connection is made (Figure 4*a*). Therefore the probability that the particle follows a given bond is proportional to the ratio of its flow rate to the total flux that goes through the connection.

The assumption of perfect mixing at each fracture node of the model must be discussed [e.g., *Krizek et al.*, 1972; *Novakowski et al.*, 1985; *Philip*, 1988; *Hull et al.*, 1987]. Practically, perfect mixing at the nodes means that all the outflows of a given fracture of the model have the same tracer concentration. In fact, according to the recent evidence of channelling [e.g. *Gentier*, 1986; *Abelin et al.*, 1985], it appears that the flow through a real fracture occurs mostly through a network of channels. The tracer mixing inside the fracture depends on the connectivity of this network and the nature of the mixing at the intersections between the flow paths. In the assumption of laminar flow, the streamlines define stream tubes with a constant flow rate [*Endo et al.*, 1984], as shown in Figure 4*b*. In the case of a dense and well-connected network of channels inside the fracture surface, the complete mixing hypothesis tends to be realistic because of the spreading of the stream tubes over all the different paths offered to the flow, thus creating an intense microscopic dispersion. Conversely, if the channel network is sparse and not connected, the tracer moves in a few preferred paths and no mixing occurs.

The particle-following method could easily take into account biased mixing or even no mixing in the fractures. But no field experiments have yet been carried out that have yielded quantitative results concerning the tracer mixing in channellized fracture flow. We therefore assumed complete mixing at the fracture nodes.

Retardation Effects Due to Tortuosity

In a given step of the particle following procedure, the particle moves along a pipe which links two nodes of the model. The pressure differences ΔH between the two nodes, the flow rate Q, and the length L of this pipe are the only data available from the hydraulic model. They are linked by the laminar flow equation $Q = K(\Delta H/L)$, where K is the equivalent hydraulic conductivity of the pipe (see paper 1). We now have to determine what residence time to assign to a particle which moves through this pipe. It is written

$$T = V/Q \tag{1}$$

where T is the particle residence time (in s), V is the volume of the pipe (in m^3), and Q is the flow rate in the pipe (in m^3 s^{-1}).

In fact, the pipe is a conceptual representation of the paths that insure the hydraulic linkage between the two nodes, i.e., the two interconnected fractures. Thus the volume V is unknown. Actually, these paths look rather like a network of small tortuous channels with large cross-section variations and dead ends [*Gentier*, 1986]. In our model we assume that the volume of these paths is proportional to the volume of a smooth and linear tube with the same hydraulic conductivity K. If the flow occurred through smooth and linear tubes, we would have, according to Poiseuille,

$$Q = \frac{\pi R^4}{8\mu}\frac{\Delta H}{L} \tag{2}$$

where R is the radius of the tube (in m), H is the pressure (in Pa), and μ is the fluid viscosity (in kg m^{-1} s^{-1}).

Thus the volume of the pipe would be

$$V = \pi R^2 L = (8\mu L^3 \pi Q/\Delta H)^{1/2} \tag{3}$$

In the model, this volume is assigned the following value:

$$V = Cr(8\mu L^3 \pi Q/\Delta H)^{1/2} \tag{4}$$

where Cr is uniform over the whole network. We call Cr the "retardation coefficient." It is very important to notice here that this retardation coefficient is related to the tortuosity of the flow paths in the fracture areas and not to chemical interactions with the matrix, such as sorption.

Hydrodynamic Dispersion Inside the Fracture Planes

The transport of solute in the fracture planes involves hydrodynamic dispersion along the pathways from one fracture to the next. This is due not only to Taylor dispersion but also to the fact that many different paths are available with various residence times for each one. We chose to take this microscopic dispersion into account to study its impact on the macroscopic dispersive behavior of the fractured system.

Although not included originally by *Robinson* [1984], longitudinal microscopic dispersion can be incorporated approximatively into the particle-following procedure by randomly modifying the average residence times at each step. In our model, the final residence time is obtained by randomly drawing the velocity deviation of the particles in a Gaussian distribution function with a mean zero and a standard deviation σ given by

$$\sigma = \frac{1}{T_m}(2U\alpha T_m)^{1/2} \tag{5}$$

where T_m is the average residence time (in s), α is the microdispersivity coefficient in the fracture plane (in m), and U is the average velocity in the pipe (in m s^{-1}).

The dispersion created in this way is an approximation of the monodimensional Fickian model of dispersion.

Both the retardation and the microdispersivity are mainly governed by the microscopic geometry of the internal faces of the fractures. Thus the local microdispersivity and the retardation coefficient are likely to be very variable from one fracture to another. The parameters α and Cr defined above are however averaged values of the local microdispersivity and retardation over the whole fracture population. It follows that α and Cr cannot easily be estimated from in situ experiments such as cross-hole tests or roughness measurements which only sample a single fracture. Too many such measurements would be required to obtain reliable estimates. Thus α and Cr are not considered as data, but as parameters of the model, and need to be calibrated.

SENSITIVITY OF THE MODEL TO ITS PARAMETERS

In this particle transport model, the particle motion is governed by the following conditions: (1) the network geometry which defines the particle paths; (2) the hydraulic properties along the particle paths, especially the fluid velocities; and (3) the two parameters associated with the

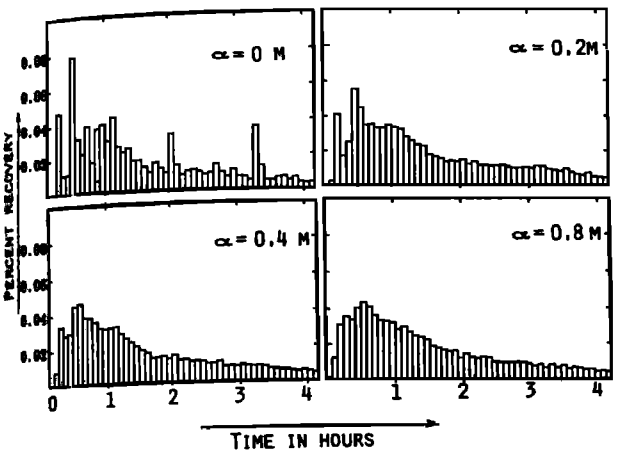

Fig. 5. Sensitivity of the model to the microscopic dispersivity.

transport model: the retardation coefficient Cr and the hydrodynamic dispersivity inside the fractures α.

In the practical application presented here, condition 1 is determined from in situ structural observations. In paper 1, we saw how condition 2 was determined by the calibration of the hydraulic conductivities on local permeability tests. In this paper, conditions 3 are the only unknowns of our problem. Before calibrating these two parameters, let us examine how they influence the transport.

Sensitivity to the Dispersion Inside the Fractures

It appears that the inclusion of microscopic dispersion leads to smooth breakthrough curves in the simulation of a tracer test. Figure 5 shows four breakthrough curves determined from 100,000 particles injected into the same network but with four different values of the microscopic dispersivity α. These breakthrough curves are histograms of the number of particles arriving at the outlet in a given mean time. The boundary conditions are represented in Figure 6. Even with α = 0.8 m which characterizes a strong dispersion, the general shape of the breakthrough curve remains the same. Thus the introduction into the model of microscopic dispersion seems to have negligible effects on the macroscopic dispersion created by the velocity differencies along the different fractures.

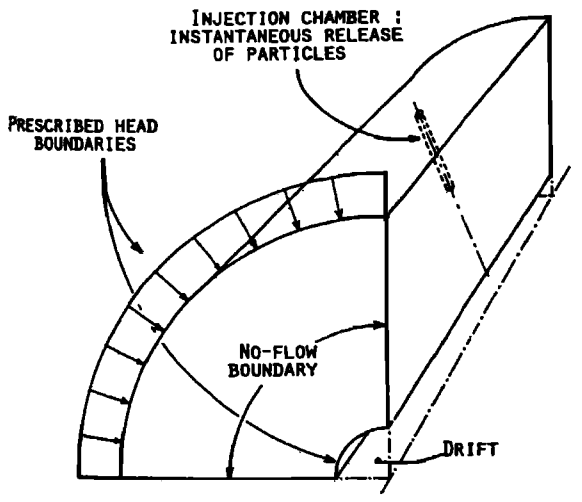

Fig. 6. Boundary conditions used for the sensitivity study.

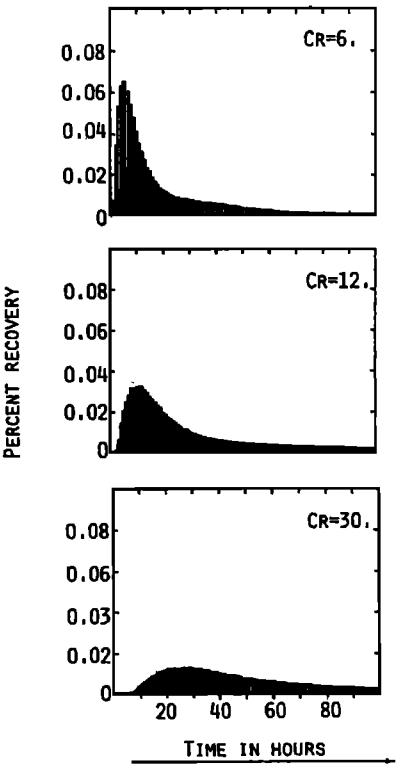

Fig. 7. Travel time histograms of 100,000 particles injected in the same network but for three different values of the retardation coefficient Cr.

Sensitivity to the Retardation Coefficient

The coefficient Cr has only a multiplicative effect on the particle residence times. It does not influence the particle trajectories nor their relative velocities in the pipes. It follows that Cr only determines the time scale of the migrations. Figure 7 shows the breakthrough curves yielded by three simulations of the injection of 100,000 particles into the same network (see the boundary conditions in Figure 6) but with three different values of Cr and a microdispersivity α = 0.8 m. The dissymmetry of these curves is due to the relative velocity discrepancies in the different flow paths. The tail represents the particles that have moved through slow channels, the peak represents the particles that have moved through high-velocity and high-flow rate channels, and the first arrival represents the particles that have taken the fastest path. The spreading of the curves is due to the retardation effect induced by Cr, but Cr does not influence the relative values of the first arrival time, peak of arrival, and breakthrough duration.

MODEL CALIBRATION

Since the transport model is not very sensitive to the microscopic dispersion, we did not try to finely adjust it on in-situ observations. The value α = 0.8 m was assigned to the microdispersivity all through the simulations, which yields smooth simulated breakthroughs like those observed in situ.

To fit the retardation coefficient, the only experimental data we have are the tracer breakthrough curves in the gallery. These tests pointed out the heterogeneity of the migration time scale at the investigated spatial scale (around 10 m). Unfortunately, we cannot quantify this heterogeneity in statistical terms, because only five of the tracer tests led to unquestionable results.

Therefore the approach used in paper 1 for calibrating the hydraulic model can no longer be used. We are faced with the following problem: our stochastic model enables us to generate an infinite number of realizations of the network surrounding each test zone. An infinity of distinct breakthrough curves is associated with this infinity of realizations. Each one could be the right one, but there is nothing to support our comparing the real experimental situation with any arbitrary one of those realizations. Neither would the assumption that each single experiment can be considered as the average response of all the realizations be justified.

Nor can we average the results of the experiments, since they are made at different distances and under different flow conditions (the flow field is not uniform around the drift, see paper 1), and furthermore, they are not numerous enough to give a meaningful average, which could be compared to an average of the realizations, using the ergodic argument. However, we can try to compare simultaneously each experimental response with the ensemble of realizations of the simulation of this particular experiment.

Our calibration procedure is then to perform a large number of realizations of each of the in-situ tracer tests, taking into account for each test the different experimental conditions. Then we adjust a single retardation coefficient for all the simulations, until we obtain, for all the experiments simultaneously, the best agreement between the observed in situ times of the peak arrival and the ones given by the simulations. The time of the peak arrival is taken as the calibration criterion since it is representative of the time scale of the migrations, which is directly determined, in the model, by the retardation coefficient.

Practically, for each simulated tracer test, the times of the peak of arrival given by the simulations are classed in a separate histogram. The Cr value is chosen so that the central part of the histograms using the same Cr value for all the calculations, is as close as possible to the in situ values of the peak time of arrival. Our underlying assumption here is that there is no reason why all the experiments should have simultaneously the same bias, and all lie on the same side of their respective distribution. With a single experiment, we could not do the calibration. With a few of them, we can do a first-order estimation. With a great number of them, this approach would be fully rigorous.

Because of the large computing efforts required, we limited ourselves to twenty realizations of each of the tracer injections in chambers 7-F2, 6-F2, 6-F3, and 4-F3 (10,000 nodes, i.e., unknowns per simulation). For the same reason, the tracer injection in chamber 3-F3 was not simulated because of the too large network involved in the test: 14,000 m^3 of rock including around 25,000 fractures. This is of course a drawback of the discrete fracture network models, which cannot represent large volumes at this stage, but it does not invalidate the methodology presented here. A larger number of tests at relatively short distances would indeed have provided a better data set for this proposed methodology.

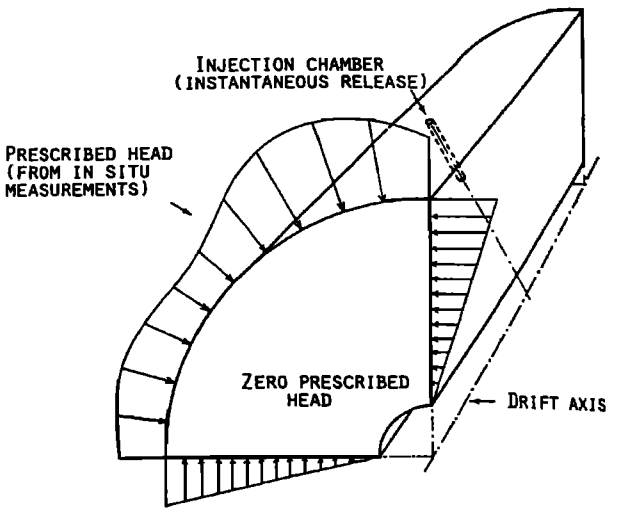

Fig. 8. Boundary conditions used for simulating the tracer injections.

The tracer tests are simulated by a pulse injection of particles in a segment that represents the injection chamber. We assume that the time between the departure of the first particle and that of the last one could be neglected compared to the breakthrough time scale, since the tracer was injected almost instantaneously in the medium (see the description of the experimental setup). The experimental conditions of the four tracer tests are precisely represented on the model, as regards both boundary conditions and geometry (see Figure 8). We emphasize that the distance between the injection chamber and the gallery is exactly the same in the model as in the real medium. Moreover, by prescribing the hydraulic pressures deduced from the measured piezometric field at the boundaries, we allow the tracer to leak outside the modeled domain, as is the case in reality.

Figure 9 shows the four histograms of the times of the peak of arrival, with $Cr = 1$. The calibrated value of Cr is calculated so as to minimize the distance:

$$\text{distance} = \sum_{i=1}^{m} \sum_{j=1}^{n} (T_i - t_{ij})^2 \tag{6}$$

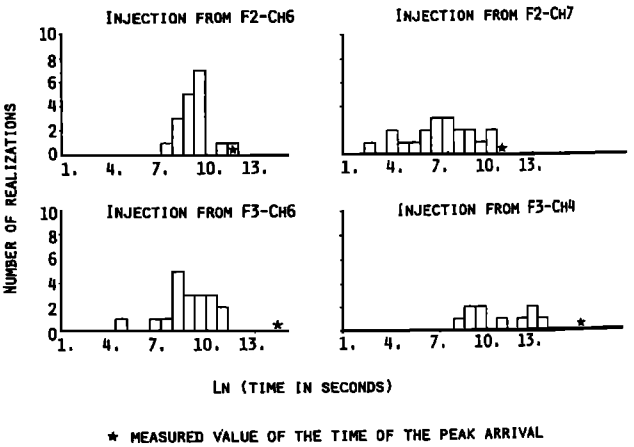

Fig. 9. Histograms of the peak arrival associated to the four sets of simulations of the tracer injections, $Cr = 1$ (before calibration).

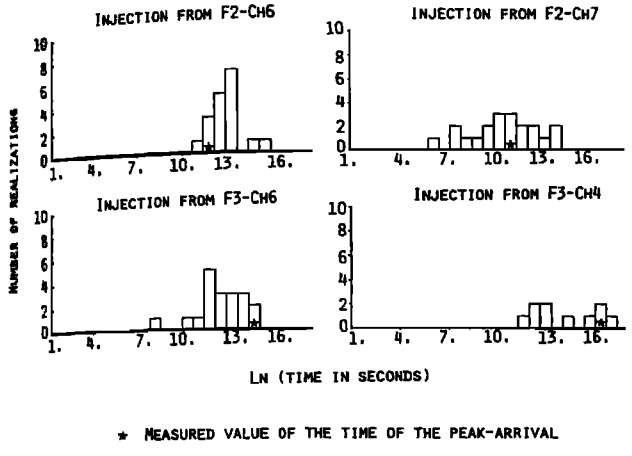

Fig. 10. Histograms of the time of the peak arrival associated to the four sets of simulations of the tracer injections, $Cr = 32$ (after calibration).

where i is the test number, T_i is the time of the peak of arrival observed in the ith test, and t_{ij} is the time of the peak of arrival of the jth simulation of the ith test.

It yields the value

$$Cr = 32$$

The four histograms of the times of the peak arrival with $Cr = 32$ are presented in Figure 10. $Cr = 32$ means that the real flow path volumes are 32 times larger on average than a smooth pipe having the same hydraulic conductivity. Let us assume for instance that these flow paths are subareas of the fracture planes, as in the case of two-dimensional flow through the fracture surface. The flow paths are then schematized by "ribbon paths" with an aperture e, a length L, and a width l. Under Poiseuille conditions, the hydraulic conductivity of this ribbon path is

$$K = e^3 l/12\mu \tag{7}$$

where K, hydraulic conductivity, is defined here as the ratio between the flow rate and the pressure gradient (in $m^4\ Pa^{-1}\ s^{-1}$), μ is the fluid viscosity (in $kg\ m^{-1}\ s^{-1}$), and e is the "ribbon path" aperture (in m).

From equation (2), the ribbon path and the smooth tube are conductivity-equivalent under the condition:

$$\pi R^4/8\mu = e^3 l/12\mu \tag{8}$$

which yields

$$R^2 = \left(\frac{2}{3\pi} e^3 l\right)^{1/2} \tag{9}$$

The volume V of the ribbon path is

$$V = elL \tag{10}$$

From equation (3), it also verifies

$$V = Cr\pi R^2 L \tag{11}$$

From equations (10) and (11), we have

$$Cr = el/\pi R^2 \tag{12}$$

and from (8),

$$Cr = \left(\frac{3l}{2\pi e}\right)^{1/2} \tag{13}$$

With $Cr = 32$, we have numerically

$$e \simeq 5 \times 10^{-4} l \tag{14}$$

From paper 1 the calibrated value of the average pipe conductivities corresponds to the radius value $R = e^{-10.4}$ m $= 3 \times 10^{-5}$ m, and from (12) and (14) we have

$$l = 0.014 \text{ m} \tag{15}$$

This result shows that under the assumption of two-dimensional laminar flow in the fractures, only narrow paths of width $l = 1.4$ cm and aperture $e = 7 \times 10^{-6}$ m can explain the observed results. Only a small portion of the fracture area is involved in the flow. This conclusion agrees with the recent observations of channelling in the fracture planes.

VALIDATION OF THE CALIBRATION OF THE CONDUCTIVITY DISPERSION

The phenomenon of macroscopic hydrodynamic dispersion is due to the spreading of the flow through a large number of different paths with different flow rates and different flow velocities. In our model, the relative flow velocities and flow rates in the pipes are determined by the hydraulic conductivities which are assigned to them. The hydrodynamic dispersion produced by the simulations is thus to a large extent determined by the initial calibration of the hydraulic model, and not by the calibration of the two parameters α and Cr of the transport model. If the transport model is able to account for the observed dispersive behavior, it will confirm the validity of the hydraulic calibration in paper 1.

Model Sensitivity to the Hydraulic Parameters

The model of the flow through the fracture network is governed by two parameters: the standard deviation σ and the mean m of the logarithm of the hydraulic conductivities which are assigned to the bonds.

The fluid velocity is proportional to the geometric mean of the hydraulic conductivities (i.e., exp (m)). Therefore the dispersivity of the medium is not modified by this parameter.

The standard deviation σ has a more specific action: it determines the range of the hydraulic conductivities, equivalent radius, and volume of the pipes that build the network. When σ is modified, the differences between the least and the most conductive bonds are changed.

To understand the consequences of this difference, let us consider a given stream tube as defined by *Endo et al.* [1984] (see Figure 4) which goes through a series of pipes. The flow rate of this stream tube approximately depends on the lowest conductivities encountered along the flow paths, whereas the residence time depends mainly on the time elapsed in the large-volume pipes. As σ increases, the highest conductivities are more and more flow contributive, whereas those with the lowest conductivities become almost noncontributive; the same thing happens to the pipe volumes, since both the hydraulic conductivity and the pipe volume are related (equation (3)). The tail of the recovery is due to the particles which are "lost" in the very slow stream tubes where the residence time is much longer than the time of the peak of

arrival. As σ increases, the percentage of these slow particles decreases because the relative flow rate that characterizes the stream tube is decreased, but the residence time is longer because the largest volumes are increased. This explains the long tail observed on the breakthrough curves. Another consequence is that most of the particles are advected through a small number of paths made only of high flow rate pipes. When σ increases, this phenomenon becomes more prevalent. σ is a factor of flow "channelling" at the scale of the flow paths. This expected sensitivity of the transport model to the parameter σ can be confirmed by particle transport simulations.

First, we simulated an injection test in the same fracture network but with three different values of the parameter σ, and the number of "contaminated" fractures was computed, defined as those through which at least one out of the 100,000 released particles is transported. The following results were obtained:

$\sigma = 1.85 \Rightarrow$ 145 contaminated fractures

$\sigma = 1 \Rightarrow$ 266 contaminated fractures

$\sigma = 0.1 \Rightarrow$ 305 contaminated fractures

The channelling phenomenon appears clearly in this result: the number of flow paths is reduced when σ increases. Note that in a real tracer experiment, all the fractures should be contaminated. Here, as a limited number of particles are put into the medium, only the fractures with the largest flow rates are contaminated. In a second test, we simulated an injection experiment in a converging flow occurring in a 1/4 cylinder of 35 m length and 14 m radius (Figure 6), with the same fracture geometry but with three different values of σ. The injection chamber is located exactly in the middle of the gallery, 12 m from the drift axis. Then, we located the breakthrough areas along the central collecting drain. The results are presented in Figure 11. In this test, almost all the particles are channelled to the same exit point when σ is large enough. Once more, the channelling phenomenon is clearly revealed.

These two tests show qualitatively how the hydraulic heterogeneities influence the particle transport in the model. Let us try to be more quantitative. The macroscopic hydrodynamic dispersion in the model is partly described by the assymmetry of the breakthrough curves. Because the probability that a particle goes through a given path is directly proportional to the flow rate in this path, the time of the peak of arrival represents the residence time corresponding to the paths with the largest flow rates. The breakthrough time for a tail concentration equal to 5% of the peak concentration is representative of the residence time in the paths with the lower flow-rates. The ratio of this time to the time of the peak of arrival is a measurement of the velocity range in the flow region. It is a good indication of the dispersive properties of the system. Therefore it seems interesting to study how it varies with σ. This is done in the following test.

Two sets of 15 planar injections are simulated in a 20 × 20 × 20 m^3 block. The flow boundary conditions are presented in Figure 12. The two sets of tests are performed with the two different values of σ: 0.1 and 1.85. Each simulation led to a time of peak arrival and a breakthrough duration as defined above. These quantities were arranged in histograms for both sets (see Figure 13). It appears that the

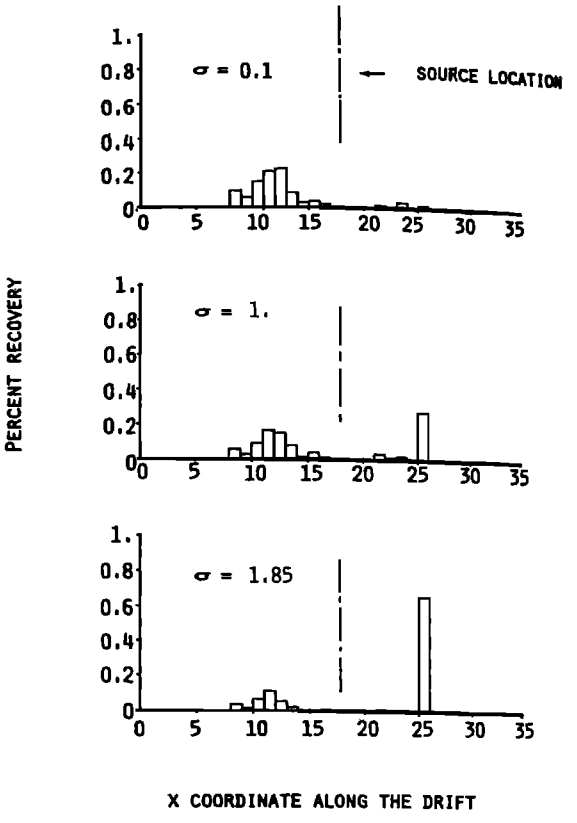

Fig. 11. Location of the recovery points along the gallery for one simulation of an injection test.

breakthrough duration is, on average, 50 times larger than the time of the peak of arrival when $\sigma = 1.85$, whereas it is only 4 times larger when $\sigma = 0.1$. The particle residence times seem to be much more dispersed for a large variance of the hydraulic conductivities than for a small one.

In conclusion to this sensitivity study, we can say that the macrodispersive properties of our particle transport model are entirely determined by the hydraulic model, especially by the standard deviation σ of the logarithm of the hydraulic conductivities assigned to the bonds linking the fracture centers.

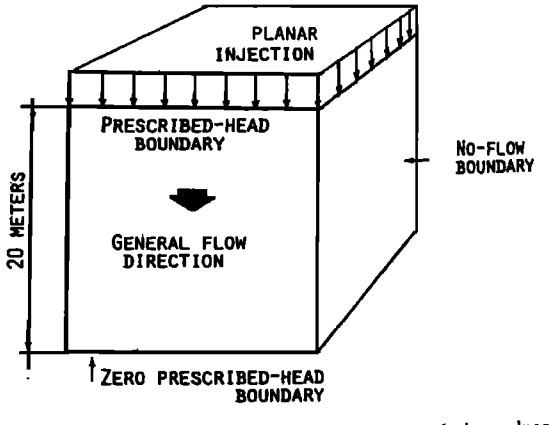

Fig. 12. Boundary conditions used to study the relative values of the peak arrival time and the breakthrough durations.

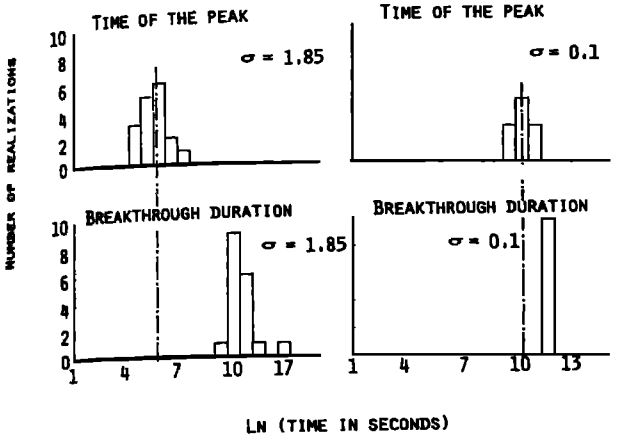

Fig. 13. Relative values of the time of the peak arrival and the breakthrough duration.

Validation Criterion

As the times of the peaks of arrival given by the model are now assumed to be calibrated, we must question whether or not the breakthrough durations given by the model fit the durations observed in the field. Once more we are facing the problem of comparing a small sample of in situ tests to an ensemble of many transport simulations performed in different realizations of the medium. The same approach as for the transport model calibration is used. We consider whether the breakthrough durations of the tracer tests are simultaneously acceptably close to the distribution of the breakthrough durations of the ensemble of realizations and of simulations of these tests. For this purpose, the breakthrough durations of the simulations corresponding to each of the four tracer tests were arranged in four histograms presented in Figure 14. Then, the observed breakthrough durations were compared to these histograms. It appears that the four experimental breakthrough durations are all included in the breakthrough duration range estimated from the simulations and reasonably close to the central value. It means that our model is able to give simultaneously satisfactory dates of the peak of arrival and of breakthrough durations without any extra calibration of the hydraulic parameter σ. This shows that the initial calibration of the hydraulic model is still appropriate for simulating the particle transport. This result appears to us as a second validation of the hydraulic model presented in paper 1 [*Cacas et al.*, this issue].

We can also try to verify if our model accounts for the low recovery rates that were observed in situ. The observed recovery rates of the four tracer tests are 45% (injection in ch7-F2), 6% (injection in ch6-F2), 14% (injection in ch6-F3), and 5% (injection in ch4-F3). The recovery rates of the simulated tracer tests lay within the large range 2–70%. Unfortunately, these recovery rates are not very meaningful in the case of our model. The calculated recovery rate only takes into account the particles which reach the collecting surface without crossing the other domain boundaries. In fact, we could imagine that some particles leak outside the domain, but return to it after a while. The recovery rate given by the model is thus underestimated. We can only conclude that the model is not inconsistent with the real system in terms of recovery rates.

Another characteristic of our model, which we could try to compare to the real system, is the concentration of the flow along a few predominant paths. This feature was shown by the study of the sensitivity to the hydraulic parameters. We saw that with a value of the standard deviation $\sigma = 1.85$ (this value corresponds to the Fanay modeling and was determined by the hydraulic calibration in paper 1) the particles concentrate in a few paths thus creating a low-density network of transport-contributive paths. This large-scale channelling phenomenon was also observed in situ at Fanay-Augères on the concentration profile (Figure 2) which shows the discontinuity of the tracer outlet along the drift. Only three tracer outlet locations could be detected. This small number of tracer outlets is also given by the simulations (Figure 11). This fact tends to prove again that the model is well adapted to the simulation of the coupled hydraulic and dispersive phenomena occurring in a fractured rock mass. A similar behavior was also observed in Stripa [*Abelin et al.*, 1985] and in Kamlunge [*Rasmuson and Neretnieks*, 1986], for instance. There is increasing evidence that regional-scale channel flow is a characteristic of flow through fractured media. Our model shows that such behavior can be explained by a strong variability in the hydraulic properties of the fracture planes.

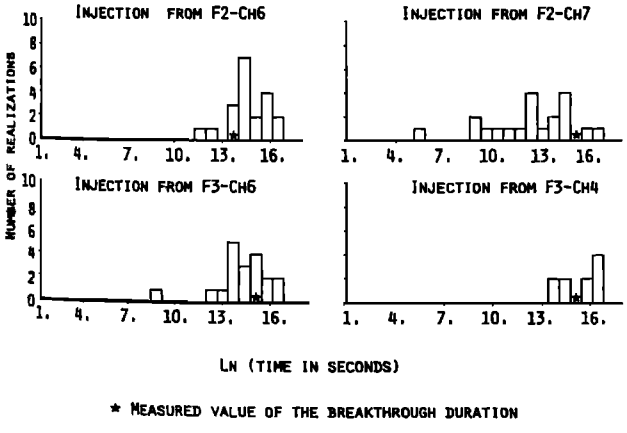

Fig. 14. Histograms of the time of the breakthrough durations associated with the four sets of simulations of the tracer injections, $Cr = 32$.

CONCLUSION

The stochastic discrete fracture network model that we have developed incorporates information on fracture geometry (inferred from fracture mapping), fracture hydraulic properties (inferred from local injection tests), and fracture transport properties (inferred from tracer tests). One essential feature of this model is that the flow in the fracture planes is assumed to be strongly channellized. Although the model is stochastic, its parameters could be calibrated from observations and experiments using ergodic assumptions to compare a large number of realizations either with a large number of independent measurements (injection tests) or with a limited number of measurements (tracer tests).

The model is capable of predicting both the regional flow properties of the medium and its variability at any scale starting from that of a single fracture.

The model structure and the calibration methodology were validated with two independent sources of information: (1)

regional hydraulic behavior (paper 1), which validates the average model conductivities; and (2) intermediate-scale tracer tests which validate the variability of the model conductivities.

The existence of flow channelling at different scales in crystalline rocks has been suggested recently [e.g., *Gentier*, 1986; *Bourke*, 1987; *Neretnieks*, 1987; *Rasmuson and Neretnieks*, 1986; *Abelin et al.*, 1985]. Our results show that it would not be realistic to interpret the tracer experiments without assuming the existence of such channels in the fracture planes. In Fanay-Augères, their dimension seems to be of the order of a few centimeters, in width, i.e., a few percent of each fracture area. Their actual shape and geometry are, however, unknown.

Acknowledgments. This work was supported by the Commission of the European Communities, the Commissariat à l'Energie Atomique, Institut de protection et de sûretè nuclèaire, and the Centre National de la Recherche Scientifique, ATP "Géotechnologies."

REFERENCES

Abelin, H., I. Neretnieks, S. Tunbrant, and L. Moreno, Migration in a single fracture: Experimental results and evaluation, final report, Stripa Proj., Stockholm, Sweden, May 1985.

Bourke, P. J., Channelling of flow through fractures in rock, report, *Ref. HL87/1124 (C22)*, Chem. Div., Harwell Lab., May 1987.

Cacas, M. C., E. Ledoux, G. de Marsily, B. Tillie, A. Barbreau, E. Durand, B. Feuga, and P. Peaudecerf, Modelling fracture flow with a stochastic discrete fracture network: Calibration and validation, 1, The flow model, *Water Resour. Res.*, this issue.

Calmels, P., B. Gaillard, and P. Margrita, Etude de l'effet d'echelle en milieu fissuré, Phase 2B, Etude des migrations, Essais de Traçages, vol. A and B, *Ref. ORIS/DAMRI/SAR/SAT/RAP/86-14/PCs*, Cent. d'Etud. Nucl. de Grenoble, Off. des Rayonnements Ionisants, Grenoble, April 1986.

Endo, H. K., J. C. S. Long, C. R. Wilson, and P. A. Witherspoon, A model for investigating mechanical transport in fracture networks, *Water Resour. Res.*, *20*(10), 1390–1400, 1984.

Gentier, S., Morphologie et comportement hydromécanique d'une fracture naturelle dans un granite sous contrainte normale: Etude expérimentale et théorique, thèse de doctorat, Univ. d'Orléans, France, March 1986.

Hull, L. C., J. D. Miller, and T. M. Clemo, Laboratory and simulation studies of solute transport in fracture networks, *Water Resour. Res.*, *23*(8), 1505–1513, 1987.

Krizek, R. J., G. M. Karadi, and E. Socias, Dispersion of a contaminant in a fissured rock, paper presented at Symposium on Percolation Through Fissured Rock, International Society of Rock Mechanics, Stuttgart, West Germany, 1972.

Neretnieks, I., Channeling in crystalline rocks: Its possible impact on transport of radionuclides from a repository, paper presented at Colloque international Impact de la physico-chimie sur l'étude, la conception et l'optimisation des procédés en milieu poreux naturel, Cent. Natl. de la Rech. Sci., Nancy, June 10–12, 1987.

Novakowski, K. S., G. V. Evans, D. A. Lever, and K. G. Raven, A field example of measuring hydrodynamic dispersion in a single fracture, *Water Resour. Res.*, *21*(8), 1165–1174, 1985.

Philip, J. R., The fluid mechanics of fracture and other junctions, *Water Resour. Res.*, *24*(2), 239–246, 1988.

Rasmuson A., and I. Neretnieks, Radionuclide transport in fast channels in crystalline rock, *Water Resour. Res.*, *22*(8), 1247–1256, 1986.

Robinson, P. C., Connectivity, flow and transport in network models of fractured media, Ph.D. thesis, St. Catherine's Coll., Oxford, Univ., Oxford, England, May 1984.

Roux, S., C. Mitescu, E. Charlaix, and C. Baudet, Letter to the editor: Transfer matrix algorithm for convection-biased diffusion, *J. Phys. A Math. Gen.*, *19*, L687–L692, 1986.

Schwartz, F. W., L. Smith, and A. S. Crowe, A stochastic analysis of macroscopic dispersion in fractured media, *Water Resour. Res.*, *19*(5), 1253–1265, 1983.

Smith, L., and F. W. Schwartz, Mass transport, 1, A stochastic analysis of macroscopic dispersion, *Water Resour. Res.*, *16*(2), 303–313, 1980.

Smith L., and F. W. Schwartz, An analysis of the influence of fracture geometry on mass transport in fractured media, *Water Resour. Res.*, *20*(9), 1241–1252, 1984.

Tsang, Y. W., and C. F. Tsang, Channel model of flow through fractured media, *Water Resour. Res.*, *23*(3), 467–479, 1987.

A. Barbreau, Commissariat à l'Energie Atomique, BP6, 92260 Fontenay aux Roses, France.

M. C. Cacas, G. de Marsily, and E. Ledoux, Ecole des Mines de Paris, 35, rue Saint-Honore, 77305 Fontainebleau, France.

P. Calmels, B. Gaillard, and R. Margritta, Centre d'Etudes Nucléaires de Grenoble, Office des Rayonnements Ionisants, BP 85x, 38041 Grenoble, France.

(Received August 22, 1988;
revised September 19, 1989;
accepted October 2, 1989.)